Random analysis on controlled buckling structure for energy harvesting

Yong Wang,[1,2] Teng Ma,[2] Hongyu Yu,[3] and Hanqing Jiang[2,a)]
[1]*Department of Engineering Mechanics, Zhejiang University, Hangzhou, Zhejiang 310027, China*
[2]*School for Engineering of Matter, Transport and Energy, Arizona State University, Tempe, Arizona 85287, USA*
[3]*School of Electrical, Computer and Energy Engineering, Arizona State University, Tempe, Arizona 85287, USA*

(Received 21 December 2012; accepted 17 January 2013; published online 1 February 2013)

The controlled buckling piezoelectric structures can be used for stretchable energy harvesting due to the stretchability and piezoelectricity. In this paper, the ambient environmental excitation is modeled as a bound-limited white noise, and the random analysis is conducted to study the system response of controlled buckling structures. The spatial distribution of the harvestable energy is revealed, and the optimal locations of electrodes for maximal energy output are indicated. The optimal locations of electrodes are robust to the upper bound of environment excitation and the applied strain. This work provides a theoretical basis for stretchable energy harvesting using controlled buckling structures. © *2013 American Institute of Physics*.
[http://dx.doi.org/10.1063/1.4789998]

Energy harvesting is to transform one type of energy, such as mechanical vibration, heat, and light, into electrical energy form by using different transduction mechanisms. Due to almost ubiquitous existing of ambient kinetic energy, much effort has been devoted to converting mechanical vibration energy into electric power by exploiting piezoelectricity,[1] electromagnetic induction,[2] or capacitance variations.[2] Because of the structural simplicity of the piezoelectric devices that only consist of piezoelectric ceramics and electrodes and their compatibility with microelectromechanical systems, piezoelectric energy harvesting devices to harness vibration energy have gained great attention. Many of these devices rely on linear resonance, and the representative geometry is a cantilever beam with piezoelectric material attached on the top or bottom surfaces of the beam.[3] The efficiency of energy harvesting using cantilever-based devices is high only in the vicinity of the system fundamental frequency but very low for other frequency ranges. To resolve the shortcoming of cantilever-based energy harvesting, some technologies has been developed, such as oscillator arrays for large frequency range coverage[4] and tunable-resonance.[5] Compared with linear resonance that has been widely used, nonlinear energy harvesting is more attractive due to the large response bandwidth and high output energy. The typical nonlinear energy harvesting includes inverted pendulum attached with permanent magnets,[6] bistable curved beams, curved shells with initial curvatures,[7] and the resonating cantilever beams attached to buckled slender bridges in which the piezoelectric cantilevers are impulsively excited when the buckled bridges snap through two equilibrium positions.[8] It has been found that superior power generation is realized by using bistable buckled beams.[9] Buckled piezoelectric beams (such as zirconate titanate,[10] aluminum nitride,[11] and zinc oxide[12]) have also been used for stretchable energy harvesting.

In this paper, we conducted random analysis for one type of buckled structure, namely, controlled buckled beams,[12] to determine the random response under the bound-limited white noise which is a reasonable approximation to ambient environment excitation. The stochastic partial differential equations were solved to obtain the system response. The results reveal the spatial distribution of the harvestable energy in ambient environment and provide the optimal locations of electrodes for maximal energy output.

The fabrication process of the controlled buckling is briefly summarized here, and the details have been presented elsewhere.[12–14] Figure 1(a) illustrates that a soft material (e.g., poly(dimethylsiloxane) (PDMS)) is subjected by a pre-strain ε_{pre} ($=\Delta L/L$ for length changed from L to $L+\Delta L$) and modified by surface treatment to define activated and inactivated regions with width W_{act} and W_{in}, respectively. The piezoelectric material (e.g., zinc oxide (ZnO)) nanoribbons are aligned parallel to the pre-strain direction on the stretched PDMS substrate (Fig. 1(b)), where the piezoelectric materials and PDMS substrate form strong and weak bonding over the activated and inactivated sites, respectively. The relaxation of the pre-strain ε_{pre} in PDMS induces the ribbons popping-up over the inactivated sites due to the interfacial delamination (Fig. 1(c)). The pop-up wavelength is given by[13] $\lambda = \frac{W_{in}}{1+\varepsilon_{pre}}$. Figure 1(d) shows a tilted view of a scanning electron microscope (SEM) image of controlled buckling ZnO ribbons with 40% pre-strain, 370 nm thickness, and $W_{act} = 40\ \mu$m, $W_{in} = 300\ \mu$m. The pop-up structure with piezoelectric materials provides a means for energy harvesting. In the following, random analysis is conducted to study the dynamic behavior of this type of structure that is buckled as the initial state.

One element of the controlled buckling structure (i.e., the popped-up region) is modeled as a fixed-fixed beam. Taking into account the geometric nonlinearity due to mid-plane stretching,[15,16] the nondimensional governing equation is given by

a)Email: hanqing.jiang@asu.edu.

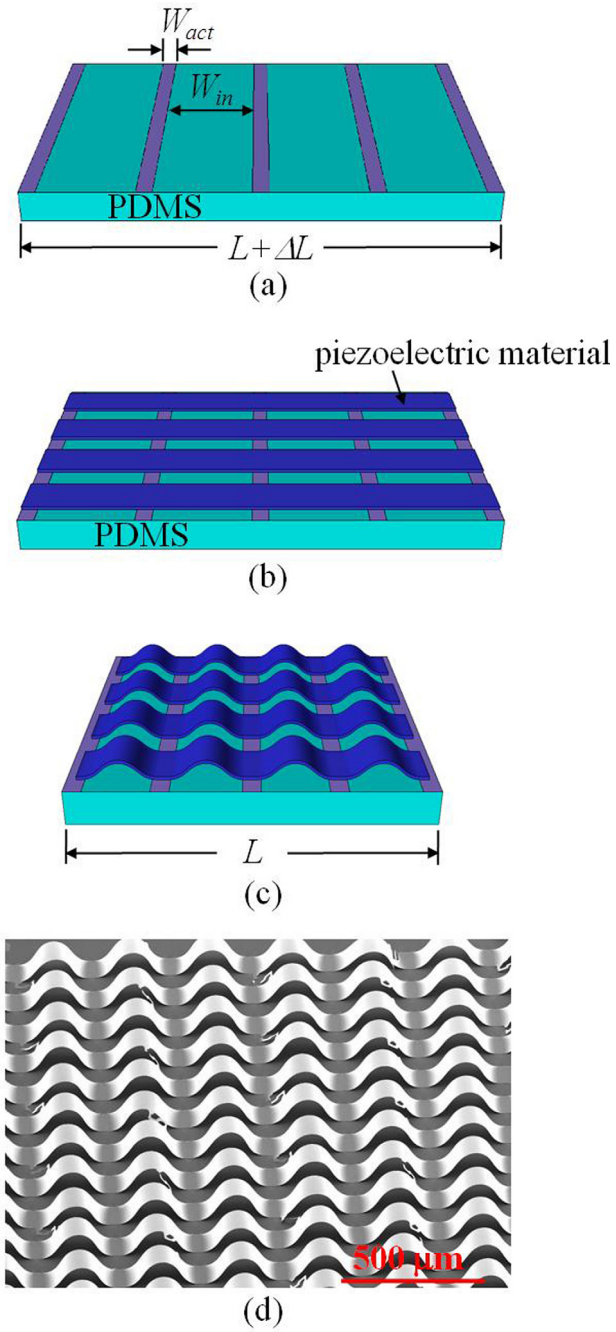

FIG. 1. Processing steps for controlled buckling piezoelectric structure on PDMS substrate. (a) Pre-strained PDMS with periodic activated and inactivated patterns. (b) Piezoelectric ribbons parallel to the pre-strain direction are attached to the pre-strained PDMS substrate. (c) The relaxation of the pre-strain in PDMS leads to buckles of piezoelectric ribbons. (d) Scanning electron microscope image of controlled buckling ZnO ribbons with 40% pres-strain, 370 nm thickness, and $W_{act} = 40\ \mu$m, $W_{in} = 300\ \mu$m.

$$\frac{\partial^2 w}{\partial t^2} + \frac{\partial^4 w}{\partial x^4} + \mu\frac{\partial w}{\partial t} + \left[\zeta_1 \frac{\varepsilon_{pre} - \varepsilon_{applied}}{1+\varepsilon_{pre}} - \frac{1}{2}\int_0^1 \left(\frac{\partial w}{\partial x}\right)^2 \mathrm{d}x\right]\frac{\partial^2 w}{\partial x^2} = F(x,t), \tag{1}$$

and the boundary conditions are

$$w = \frac{\partial w}{\partial x} = 0, \quad \text{at} \quad x = 0, 1. \tag{2}$$

Here the nondimensional spatial coordinate, time, and transverse deflection are defined as $x = \hat{x}/W_{in}$, $t = \hat{t}\sqrt{E/(12\rho)}h/W_{in}^2$, and $w = \sqrt{12}\hat{w}/h$, in which $\hat{x}$, $\hat{t}$, and $\hat{w}$ are the dimensional spatial coordinate along with the ribbon direction, time, and the transverse deflection, respectively. E, ρ, and h are the Young's modulus, density, and thickness of the piezoelectric material, respectively. Other nondimensional variables are $\mu = \hat{\mu}W_{in}^2/(bh^2\sqrt{\rho E/12})$, $F = 24\sqrt{3}\hat{F}W_{in}^4/(Ebh^4)$, and $\zeta_1 = 12W_{in}^2/h^2$, in which $\hat{\mu}$, $\hat{F}$ are the damping coefficient and the distributed load and b is the ribbon width. $\varepsilon_{applied}$ denotes the applied strain exerted on PDMS substrate after relaxation of ε_{pre}. In Eq. (1), the square bracket term shows the effect of mid-plane stretching, and the right hand side means random excitation.

By dropping the time-dependent terms in Eq. (1), one arrives at a static solution, which gives the postbuckling configuration with respect to applied strain $\varepsilon_{applied}$,[16]

$$w_{static}(x) = 2\sqrt{\frac{\varepsilon_{pre} - \varepsilon_{applied}}{(1+\varepsilon_{pre})\varepsilon_{cr}} - 1}[1 - \cos(2\pi x)], \tag{3}$$

where $\varepsilon_{cr} = \frac{\pi^2}{3}\left(\frac{h}{W_{in}}\right)^2$ is the critical buckling strain. To obtain the vibration modes, the damping term (i.e., $\mu\frac{\partial w}{\partial t}$) and the excitation term (i.e., F term) are neglected, and a small disturbance around the static postbuckling configuration $w_{static}(x)$ is introduced as $v(x,t) = w(x,t) - w_{static}(x)$. The governing equation and the corresponding boundary conditions with respect to the small disturbance are given by

$$\begin{aligned} \frac{\partial^2 v}{\partial t^2} + \frac{\partial^4 v}{\partial x^4} + 4\pi^2\frac{\partial^2 v}{\partial x^2} &= \frac{\partial^2 w}{\partial x^2}\int_0^1 \frac{\partial v}{\partial x}\frac{\partial w_{static}}{\partial x}\mathrm{d}x, \\ v = \frac{\partial v}{\partial x} &= 0, \quad \text{at} \quad x = 0, 1. \end{aligned} \tag{4}$$

Using the method of separation of variables, i.e., $v(x,t) = V(x)T(t)$, the solution of the space function $V(x)$ can be expressed as

$$\begin{aligned} V(x) = d_1\sin(s_1 x) + d_2\cos(s_1 x) + d_3\sinh(s_2 x) \\ + d_4\cosh(s_2 x) + d_5\frac{\partial^2 w_{static}}{\partial x^2}, \end{aligned} \tag{5}$$

where $s_{1,2} = \sqrt{\pm 2\pi^2 + \sqrt{4\pi^4 + \omega^2}}$, $\omega = \frac{\Omega}{\sqrt{\frac{E}{12\rho}}\frac{h}{W_{in}^2}}$ is the nondimensional natural frequency, and Ω is the dimensional natural frequency. The relation between d_5 and $d_i (i = 1 \sim 4)$ is $\left\{\omega^2 - 32\pi^4\left[\frac{\varepsilon_{pre}-\varepsilon_{applied}}{(1+\varepsilon_{pre})\varepsilon_{cr}} - 1\right]\right\}d_5 + \int_0^1\left(\frac{\partial V}{\partial x} - d_5\frac{\partial^3 w_{static}}{\partial x^3}\right)\frac{\partial w_{static}}{\partial x}\mathrm{d}x = 0$. Combining these relations and the boundary condition (Eq. (4)), one determines the constants $d_i (i = 1, 2, ..., 5)$, as well as the nondimensional natural frequencies $\omega_i (i = 1, 2, ...)$ and the corresponding modal shapes around the static postbuckling configuration $w_{static}(x)$.

Figure 2 shows the results of the first four modal shapes and the postbuckling after disturbance around the static postbuckling configurations $w_{static}(x)$ for $\frac{\varepsilon_{pre}-\varepsilon_{applied}}{(1+\varepsilon_{pre})\varepsilon_{cr}} = 2 \times 10^4$. The natural frequencies show insensitivity to the pre- and applied strains, since $\omega_1 = 44.36$, $\omega_2 \in [73.39, 74.38]$, $\omega_3 = 182.12$, and $\omega_4 \in [251.82, 259.45]$ for $(\varepsilon_{pre} - \varepsilon_{applied})/[(1+\varepsilon_{pre})\varepsilon_{cr}] \in [10^2,\ 10^6]$. It is also noticed that the first-order

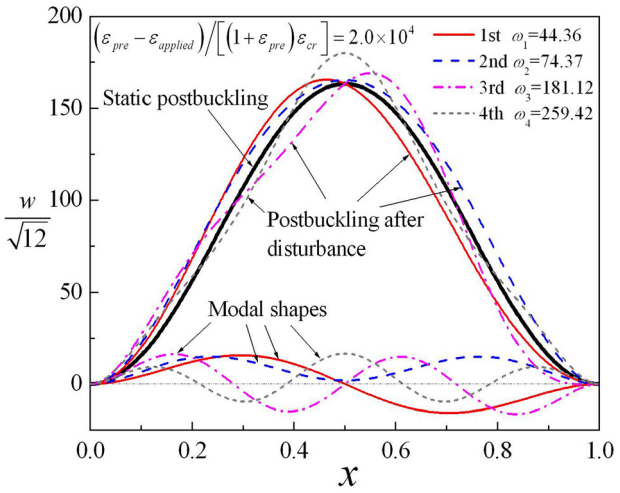

FIG. 2. Analytical results of the first four-order modal shapes of controlled buckling structure.

and third-order modal shapes are asymmetric while the second-order and fourth-order modal shapes are symmetric. This phenomenon apparently distinguishes with that of the planar beam and will induce the singular random behaviors of the controlled buckling structure as to be discussed in the following.

Now the external excitation term $F(x,t)$ and the damping term in Eq. (1) are considered. The external excitation $F(x,t)$ is assumed to be spatially homogenous when the source of excitation is far away from the controlled buckling structure that are on the order of micrometers and varies with time t, i.e., $F(x,t)=f\xi(t)$, where f is the excitation amplitude and $\xi(t)$ is a bound-limited white noise with correlation function $R_\xi(\tau)$ and power spectrum density $S_\xi(\omega)$.[17] Under random excitation, a disturbance $v(x,t)$ is induced and can be expanded by modal shapes[18] $v(x,t)=\mathbf{V}^T(x)\cdot\mathbf{T}(t)$, where the bold symbols are for matrixes. Substituting the expanded disturbance into the governing equation (4) and utilizing the orthogonal properties of modal shapes, one arrives at

$$\mathbf{a}\cdot\frac{d^2\mathbf{T}}{dt^2}+\mathbf{b}\cdot\frac{d\mathbf{T}}{dt}+\mathbf{c}\cdot\mathbf{T}=\mathbf{d}\xi(t), \tag{6}$$

where $\mathbf{a}$, $\mathbf{b}$, $\mathbf{c}$, and $\mathbf{d}$ are matrixes expressed in terms of modal shapes. The power spectrum density matrix of $\mathbf{T}(t)$ is $\mathbf{S_T}(\omega)=\bar{\mathbf{H}}(\omega)\cdot\mathbf{H}^T(\omega)S_\xi(\omega)$, where $\mathbf{H}(\omega)=(-\omega^2\mathbf{a}+i\omega\mathbf{b}+\mathbf{c})^{-1}\cdot\mathbf{d}$ is the frequency response function, i is the imaginary unit, and the superscripts "*bar*" and "*T*" denote the conjugate and transpose, respectively. Therefore, the power spectrum density of the disturbance $v(x,t)$ can be expressed as

$$S_v(x,\omega)=\mathbf{V}^T(x)\cdot\bar{\mathbf{H}}(\omega)\cdot\mathbf{H}^T(\omega)\cdot\mathbf{V}(x)S_\xi(\omega). \tag{7}$$

The mean-square value of the disturbance $v(x,t)$ can be expressed through the integration of the associated power spectrum density, i.e., $E[v^2]=\int_{-\infty}^{\infty}S_v(x,\omega)\mathrm{d}\omega$.

The disturbance caused by random excitation changes the bending curvature and the maximal change of the axial strain is proportional to curvature change, given by $\Delta\varepsilon_{\max}=\frac{h}{2}\left(\frac{\partial^2 v}{\partial x^2}\right)_{\max}$. The expectation of the change of axial strain under random vibration provides a means to evaluate the location of maximum harvestable bending energy, which is practically important for energy harvesting using pop-up buckling structures. From Eq. (7), the power spectrum density and the mean-square value of the curvature change $\frac{\partial^2 v}{\partial x^2}$ are given by

$$\begin{aligned}S_{v''}(x,\omega)&=\frac{d^2\mathbf{V}^T}{dx^2}\cdot\bar{\mathbf{H}}(\omega)\cdot\mathbf{H}^T(\omega)\cdot\frac{d^2\mathbf{V}}{dx^2}S_\xi(\omega)\\ E[v''^2]&=\int_{-\infty}^{\infty}S_{v''}(x,\omega)\mathrm{d}\omega.\end{aligned} \tag{8}$$

Figure 3(a) shows the power spectrum densities of the disturbance $S_v(x,\omega)$ and the curvature change $S_{v''}(x,\omega)$ at $x=0.25$ normalized by that of the excitation $S_\xi(\omega)$ for $\mu=0.1$, excitation constant $f=1$, and $(\varepsilon_{pre}-\varepsilon_{applied})/[(1+\varepsilon_{pre})\varepsilon_{cr}]=2.0\times10^4$. It is found that there are peaks at $\omega=\omega_2,\omega_4$ but no peaks at $\omega=\omega_1,\omega_3$, because the first-order and the third-order modal shapes are asymmetric as

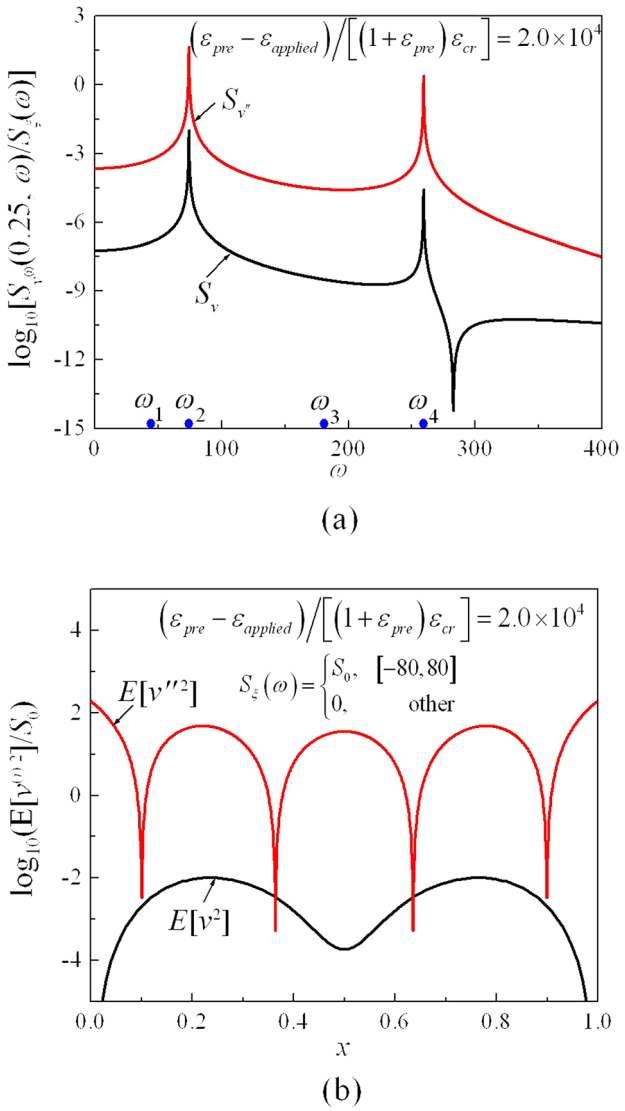

FIG. 3. Random analysis results. (a) The power spectrum densities of the disturbance $S_v(x_1,\omega)$ and the curvature change $S_{v''}(x_1,\omega)$ at $x_1=0.25$, normalized by that of the excitation $S_\xi(\omega)$, as functions of ω. (b) The mean-square values of the disturbance $E[v^2]$ and curvature change $E[v''^2]$, normalized by S_0, as functions of x.

shown in Fig. 2 and almost cannot be excited by the uniform-distribution mono-source excitation.

Suppose the power spectrum density of bound-limited white noise $\xi(t)$ is

$$S_\xi(\omega) = \begin{cases} S_0, & [-80, 80] \\ 0, & \text{other} \end{cases}. \tag{9}$$

The mean-square values of the disturbance $E[v^2]$ and curvature change $E[v''^2]$, normalized by S_0, are shown in Fig. 3(b). It is found that the mean-square values ($E[v^2]$ and $E[v''^2]$) are symmetric about the center. The maximal mean-square value of curvature change ($E[v''^2]$) appears at $x = 0, 1$ and three extreme values appear at $x = 0.220, 0.780$, and $x = 1/2$, in which the value at $x = 0.220, 0.780$ is larger than that at $x = 1/2$. For large energy output, the electrode should be placed at the locations with maximal curvature changes. These results suggest that the optimal locations of the electrode are the anchor points between the activated and inactivated areas (i.e., $x = 0, 1$), and the sub-optimal locations are $x = 0.220, 0.780$.

We also studied the effects of band-width of external excitation and the applied strain on the optimal locations of electrodes. The dependences of the optimal locations of electrodes and the extreme values of mean-square value of curvature change on the upper bound ω_{upper} of external excitation are shown in Fig. 4, where the upper bound ω_{upper} is limited in the interval [5, 100]. Figure 4(a) shows the relation between the optimal locations of electrodes and the upper bound ω_{upper}, where only half length of the beam is shown due to the symmetry of the optimal locations. It is observed that the first and the third optimal locations keep constant (0, and 1/2), while the second optimal locations vary slightly upon the upper bound ω_{upper} (in the ranges [0.207, 0.220]). This result indicates that the robustness of the optimal locations of electrodes on the upper bound of external excitation and the conclusion in Fig. 3(b) holds for a wide range of frequency. Figure 4(b) shows the relation of the extreme values of mean-square value of curvature change $E[v''^2]$ to the upper bound ω_{upper}. It is found that the harvestable energy increases significantly as the upper bound ω_{upper} passes the second fundamental natural frequency ω_2 and then keeps constant for further increase of the upper bound.

The dependences of the optimal locations of electrodes and the extreme values of mean-square value of curvature change on applied strain are studied for two representative excitations, $\omega_{upper} = 80 > \omega_2$ and $\omega_{upper} = 60 < \omega_2$, and the applied strain is limited in the interval $(\varepsilon_{pre} - \varepsilon_{applied})/[(1 + \varepsilon_{pre})\varepsilon_{cr}] \in [10^2, 10^6]$. Figure 4(c) shows the relation between the optimal locations and the applied strain, in which the first and the third optimal location keep constant (0 and 1/2), while the second optimal location slightly changes from 0.221 to 0.220 for $\omega_{upper} = 80$ and from 0.212 to 0.211 for $\omega_{upper} = 60$. Figure 4(d) shows the dependency of $\log_{10}(E[v''^2]/S_0)$ on applied strain for $\omega_{upper} = 80$ and 60. Once again, it is found that the dependency on applied strain is weak but strong on ω_{upper}, which is consistent with Fig. 4(b).

The random response of controlled buckling structure subject to the bound-limited white noise is studied in this paper. The spatial distribution of the harvestable energy is revealed and the optimal locations of electrodes for maximal

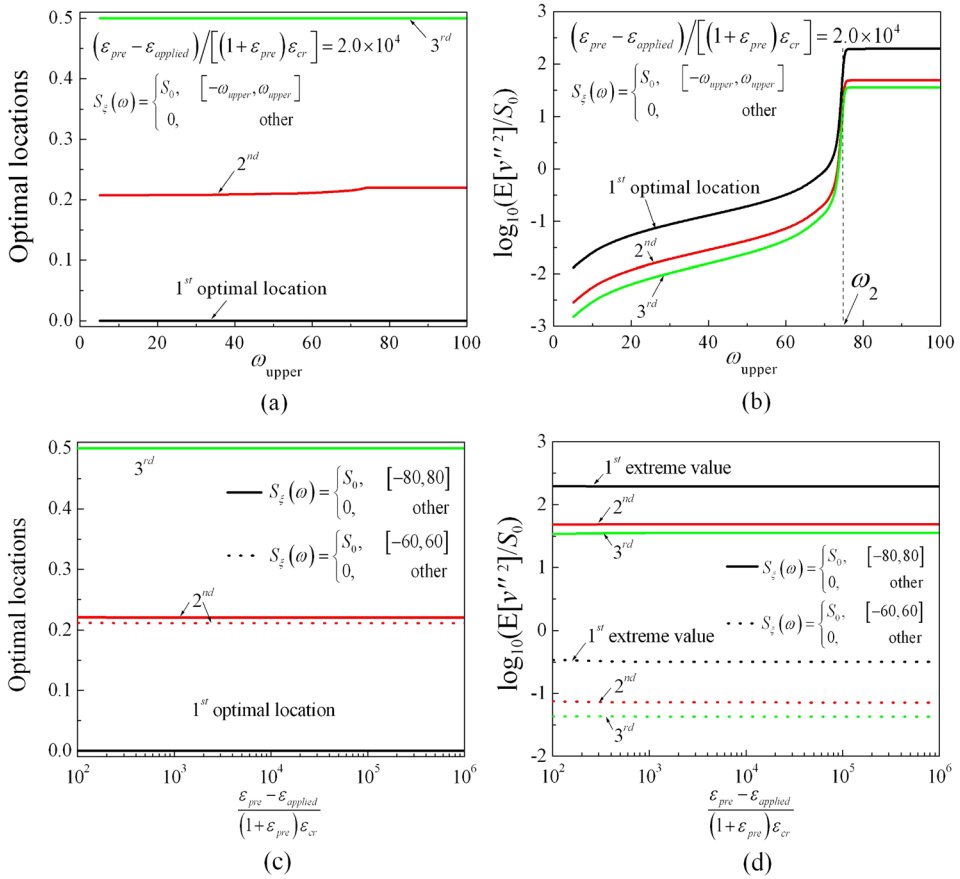

FIG. 4. Effects of ω_{upper} and applied strain. (a) The dependence of the optimal locations of electrodes on the upper bound ω_{upper} of environment excitation. (b) The dependence of the extreme values of mean-square value of curvature change on the upper bound ω_{upper} of environment excitation. (c) The dependence of the optimal locations of electrodes on the applied strain for $\omega_{upper} = 80$ and 60. (d) The dependence of the extreme values of mean-square value of curvature change on the applied strain for $\omega_{upper} = 80$ and 60.

energy output are indicated. The optimal locations of electrodes are robust to the upper bound of environment excitation and the applied strain. This work provides a theoretical basis to use the pop-up structures for stretchable energy harvesting device. It is noticed that although the present study does not consider the electrodes that are indispensable in real device, the approach used in this analysis also holds for multilayer structures by simply using the equivalent material properties.

Y.W. acknowledges the National Natural Science Foundation of China under Grant No. 11002077. T.M. acknowledges the financial support from the China Scholarship Council. H.Y. acknowledges the support from NSF CMMI-0928502. H.J. acknowledges the support from NSF CMMI-0700440 and CMMI-0928502.

[1]M. Umeda, K. Nakamura, and S. Ueha, Jpn. J. Appl. Phys., Part 1 **35**, 3267 (1996); S. R. Anton and H. A. Sodano, Smart Mater. Struct. **16**, R1 (2007).
[2]M. Mizuno and D. G. Chetwynd, J. Micromech. Microeng. **13**, 209 (2003).
[3]S. P. Beeby, M. J. Tudor, and N. M. White, Meas. Sci. Technol. **17**, R175 (2006); N. M. White, P. Glynne-Jones, and S. P. Beeby, Smart Mater. Struct. **10**, 850 (2001); S. Roundy and P. K. Wright, Smart Mater. Struct. **13**, 1131 (2004).
[4]I. Sari, T. Balkan, and H. Kulah, presented at the Solid-State Sensors, Actuators and Microsystems Conference, 10–14 June 2007; H. U. Kim, W. H. Lee, H. V. R. Dias, and S. Priya, IEEE Trans. Ultrason. Ferroelectr. Freq. Control **56**, 1555 (2009); D. B. Zhu, M. J. Tudor, and S. P. Beeby, Meas. Sci. Technol. **21**, 022001 (2010).
[5]E. S. Leland and P. K. Wright, Smart Mater. Struct. **15**, 1413 (2006); R. Masana and M. F. Daqaq, Trans. ASME, J. Vib. Acoust. **133**, 011007 (2011).
[6]F. Cottone, H. Vocca, and L. Gammaitoni, Phys. Rev. Lett. **102**, 080601 (2009); N. A. Khovanova and I. A. Khovanov, Appl. Phys. Lett. **99**, 144101 (2011).
[7]J. Casals-Terre, A. Fargas-Marques, and A. M. Shkel, J. Microelectromech. Syst. **17**, 1082 (2008); A. F. Arrieta, P. Hagedorn, A. Erturk, and D. J. Inman, Appl. Phys. Lett. **97**, 104102 (2010).
[8]S. M. Jung and K. S. Yun, Appl. Phys. Lett. **96**, 111906 (2010).
[9]F. Cottone, L. Gammaitoni, H. Vocca, M. Ferrari, and V. Ferrari, Smart Mater. Struct. **21**, 035021 (2012).
[10]Y. Qi, J. Kim, T. D. Nguyen, B. Lisko, P. K. Purohit, and M. C. McAlpine, Nano Lett. **11**, 1331 (2011).
[11]H. C. Seo, I. Petrov, H. Jeong, P. Chapman, and K. Kim, Appl. Phys. Lett. **94**, 092104 (2009).
[12]T. Ma, Y. Wang, R. Tang, H. Yu, and H. Jiang, "Pre-patterned ZnO nanoribbons on soft substrates for stretchable energy harvesting applications" (unpublished).
[13]H. Jiang, Y. Sun, J. A. Rogers, and Y. Y. Huang, Appl. Phys. Lett. **90**, 133119 (2007).
[14]Y. G. Sun, W. M. Choi, H. Q. Jiang, Y. G. Y. Huang, and J. A. Rogers, Nat. Nanotechnol. **1**, 201 (2006).
[15]A. H. Nayfeh and P. F. Pai, *Linear and Nonlinear Structural Mechanics* (Wiley, New York, 2004).
[16]A. H. Nayfeh and S. A. Emam, Nonlinear Dyn. **54**, 395 (2008).
[17]E. Wong and B. Hajek, *Stochastic Processes in Engineering Systems* (Springer, New York, 1985).
[18]Y. K. Lin, *Probabilistic Theory of Structural Dynamics* (McGraw-Hill Book Company, New York, 1967).